Bone Marrow–Derived Cell Recruitment to the Neurosensory Retina and Retinal Pigment Epithelial Cell Layer Following Subthreshold Retinal Phototherapy

Sergio Caballero,[1] David L. Kent,[2] Nilanjana Sengupta,[1] Sergio Li Calzi,[3] Lynn Shaw,[3] Eleni Beli,[3] Leni Moldovan,[3] James M. Dominguez II,[4] Ramana S. Moorthy,[5] and Maria B. Grant[3]

[1]Pharmacology and Therapeutics, University of Florida, Gainesville, Florida, United States
[2]The Vision Clinic, Kilkenny, Ireland
[3]Eugene and Marilyn Glick Eye Institute, Indiana University School of Medicine, Indianapolis, Indiana, United States
[4]Department of Medicine, Indiana University School of Medicine, Indianapolis, Indiana, United States
[5]AVRUC, Indiana University Medical Center, Indianapolis, Indiana, United States

Correspondence: Maria B. Grant, Walther Hall Research Building 3, 980 West Walnut Street, Indianapolis, IN 46202, USA; mabgrant@iupui.edu.

Submitted: September 12, 2016
Accepted: June 16, 2017

Citation: Caballero S, Kent DL, Sengupta N, et al. Bone marrow–derived cell recruitment to the neurosensory retina and retinal pigment epithelial cell layer following subthreshold retinal phototherapy. *Invest Ophthalmol Vis Sci*. 2017;58:5164–5176. DOI: 10.1167/iovs.16-20736

Purpose. We investigated whether subthreshold retinal phototherapy (SRPT) was associated with recruitment of bone marrow (BM)–derived cells to the neurosensory retina (NSR) and RPE layer.

Methods. GFP chimeric mice and wild-type (WT) mice were subjected to SRPT using a slit-lamp infrared laser. Duty cycles of 5%, 10%, 15%, and 20% (0.1 seconds, 250 mW, spot size 50 μm) with 30 applications were placed 50 to 100 μm from the optic disc. In adoptive transfer studies, GFP^+ cells were given intravenously immediately after WT mice received SRPT. Immunohistochemistry was done for ionized calcium-binding adapter molecule-1 ($IBA\text{-}1^+$), CD45, Griffonia simplicifolia lectin isolectin B4, GFP or cytokeratin). Expression of *Ccl2*, *Il1b*, *Il6*, *Hspa1a, Hsp90aa1*, *Cryab*, *Hif1a*, *Cxcl12*, and *Cxcr4* mRNA and flow cytometry of the NSR and RPE-choroid were performed.

Results. Within 12 to 24 hours of SRPT, monocytes were detected in the NSR and RPE-choroid. Detection of reparative progenitors in the RPE occurred at 2 weeks using flow cytometry. Recruitment of GFP^+ cells to the RPE layer occurred in a duty cycle–dependent manner in chimeric mice and in mice undergoing adoptive transfer. *Hspa1a*, *Hsp90aa1*, and *Cryab* mRNAs increased in the NSR at 2 hours post laser; *Hif1a*, *Cxcl12*, *Hspa1a* increased at 4 hours in the RPE-choroid; and *Ccl2*, *Il1b*, *Ifng*, and *Il6* increased at 12 to 24 hours in the RPE-choroid.

Conclusions. SRPT induces monocyte recruitment to the RPE followed by hematopoietic progenitor cell homing at 2 weeks. Recruitment occurs in a duty cycle–dependent manner and potentially could contribute to the therapeutic efficacy of SRPT.

Keywords: micropulse, subthreshold, macular edema

AMD is the most common cause of blindness in the Western world. As a consequence, this disease is considered a major public health problem. Approximately 85% to 90% of individuals have the nonexudative form of AMD. This consists of RPE loss, atrophy, and depigmentation. With the exception of dietary supplements, there is no effective treatment available.[1,2] New therapies are therefore urgently required to treat this rapidly growing population of individuals. One therapeutic approach not yet fully evaluated for nonexudative AMD is cellular therapeutics. The bone marrow (BM) is an accessible source of progenitor cells and reparative cells.[3–6] These cells can home to areas of injury, participate with resident cells in repair of diseased tissues, and when in the circulation, are amenable to both hormonal and pharmacological manipulation. In earlier studies, using GFP chimeric mice in the laser-induced model of choroidal neovascularization (CNV), we demonstrated recruitment of BM cells to areas of damaged retina and choroid.[7–9] Using sodium iodate to induce RPE injury, we demonstrated that BM-derived cells are mobilized to the RPE layer and associate with the remaining RPE cells to promote proper RPE repair.[8,10]

BM stem/progenitor cells have been used to treat individuals with retinal or neurologic diseases.[11–14] The major protective mechanism of these cells is their paracrine secretion of factors with anti-inflammatory, antiapoptotic, proliferative, and proangiogenic actions.[15,16] However, the BM is also a source of inflammatory cells, which can infiltrate into the retina or brain parenchyma in response to alterations that may occur after injury.[17–21] Proinflammatory cells can contribute to both physiological repair and pathophysiological events, including cytokine release.[22] Extravasation of BM-derived cells into the central nervous system and the retina contribute to the generation of microglia identified using IBA-1 immunohistochemistry. Typically at the site of injury, the number of microglia that originates from BM increases dramatically after tissue damage.[23] We have observed this paradigm for retinal damage induced by diabetes.[19,24–27] The capacity of microglial precursors to cross the blood–brain barrier and home to sites of

neural damage and inflammation makes these cells particularly useful for therapeutic strategies in the retina and brain.

Continuous wave (CW) thermal lasers have long been important tools for the treatment of various retinal disorders.[28–33] Their therapeutic efficacy in the treatment of diabetic macular edema (DME) is well-established but at the expense of potentially serious side effects such as development of scotomata, subretinal scarring, and CNV, all resulting from thermal-induced damage to the outer retina, RPE, and Bruch's membrane.[30,34–41] However, the precise mechanism of action of CW laser has yet to be fully delineated.[42–51]

Recently developed to minimize photothermal damage to the retina and adjacent structures, micropulse laser induces photochemical injury.[52–56] In this study, we investigated the migration and microglial nature of BM-derived cells present in the neurosensory retina (NSR) and RPE-choroid at various time points after subthreshold retinal phototherapy (SRPT) using various duty cycles (DCs).

Methods

Animals

All animal studies were approved by the Institutional Animal Care and Use Committee at the University of Florida and Indiana University, and studies were conducted in accordance with the principles described in the ARVO Statement for the Use of Animals in Ophthalmic and Vision Research.

To facilitate the identification of BM-derived cells, GFP BM chimeric mice were generated. Adult (12 weeks) C57BL-6J female mice were irradiated (950 rads) to ablate their BM. Immediately after irradiation, they were given 10,000 cKit$^+$Sca-1$^+$ BM stem cells obtained from 12-week-old male C57BL/6-Tg (ACTB-EGFP) transgenic mice as previously described.[9] Animals were assessed for BM reconstitution 4 weeks after transplant by determining the percentage of peripheral blood leukocytes (PBLs) expressing GFP. Those animals with at least 80% of PBLs positive for GFP were considered fully reconstituted and used for subsequent experiments.

BM Cell Recruitment Following SRPT

We assessed the degree of microglial activation in the retina by measuring the relative expression of IBA-1 (a marker for microglia) at various times following SRPT. Each mouse received 10% DC SRPT in one eye for 0.1 seconds at 250 mW and a spot size set to 50 μm. Thirty applications were administered to each eye circumferentially placed between 50 and 100 μm from the optic disc. Eyes were then harvested at 0 (control, no laser), 12 hours, 24 hours, and 2 weeks ($n = 5$ animals per time point and repeated in triplicate). Harvested eyes were dehydrated, embedded in paraffin, and sectioned (6-μm sections, collecting every third section). After deparaffination, the sections were incubated with goat anti–IBA-1 (Wako, Richmond, VA, USA) followed by Alexa Fluor 647–conjugated second antibody (Abcam, Cambridge, MA, USA), mounted with DAPI antifade medium (Vector Laboratories, Burlingame, VT, USA), and imaged using a Leica laser scanning spectral confocal microscope (TCS-SP2; Leica, Buffalo Grove, IL, USA).

Another set of eyes from wild-type (WT) mice was fixed in buffered 4% (wt/vol) paraformaldehyde overnight at 4°C, then washed by immersion in two changes of PBS before dissection. Neural retina was discarded, and posterior segment was permeabilized and blocked overnight at 4°C in PBS containing 0.3% (vol/vol) Triton X-100 and 0.2% (wt/vol) bovine serum albumin (Sigma-Aldrich Corp., St. Louis, MO, USA) and 5% goat serum in 10 mM HEPES buffer. Samples were then incubated overnight at 4°C in either rabbit anti-Occludin (Zymed, South San Francisco, CA, USA) diluted 1:50; rat anti-CD45 (Novus Biologicals, Littleton, CO, USA) diluted 1:10; or fluorescein-labeled *Griffonia simplicifolia* lectin isolectin B4 (Vector Laboratories) in blocking buffer. After washes in two changes of PBS, samples were incubated in goat anti-rabbit Dylight 649 (Abcam) diluted 1:200 and/or goat anti-rat Dylight 488 (ThermoFisher, Waltham, MA, USA) diluted 1:200 for 4 hours at 4°C. After performing five radial incisions, posterior segments were flat-mounted on a glass slide, and antifade medium (Vectashield; Vector Laboratories) and glass coverslips were applied. Digital image captures (~3 μm z-depth) were made using a laser scanning confocal microscope Z-series captures (Zeiss, Thornwood, NY, USA).

Preparation of NSR and RPE—Choroid Into a Single-Cell Suspension

From representative eyes, the NSR and the RPE-choroid were dissected and placed in RPMI-1640 (Sigma-Aldrich Corp.) supplemented with 5% fetal bovine serum (FBS). NSRs were then digested in 1 mL RPMI-5% FBS with 0.5 mg/mL collagenase D (Roche, Indianapolis, IN, USA) and 250 μg/mL DNAse (Sigma-Aldrich Corp.) for 30 minutes at 37°C after disrupting the tissue with a pipette in a microcentrifuge tube. RPE-choroid was digested in 1 mL RPMI-5% FBS with 0.5 mg/mL collagenase D and 250 μg/mL DNAse for 30 minutes at 37°C after cutting the tissue with scissors. Single-cell suspensions were generated, and the digested tissue segments were passed through a 70-μm cell strainer with the plunger of a 3-mL syringe. Cells were washed twice with PBS-2% FBS supplemented with 1 mM EDTA (fluorescence-activated cell sorting [FACS] buffer). The single-cell suspensions of NSR and RPE-choroid from each eye were stained with antibodies for flow cytometry as described in the following sections.

Flow Cytometry and FACS Analysis

Cells were incubated for 10 minutes on ice with 20 μg/mL TruStain fcX 93 (Biolegend, San Diego, CA, USA) for nonspecific binding. Subsequently, cells were stained for 30 minutes and placed on ice with combinations of the following antibodies: (1) for myeloid cells: FITC-Ly6C, HK1.4 (Biolegend); PE-Ly6G, 1A8; PECy7-CD11c, HL3; PE-CF594-CD11b, M1/70; Alexa Fluor 700-CD45, 30-F11; V500-CD3e, 500A2; BV-421-NK1.1, PK136 (BD Bioscience, San Jose, CA, USA); APC-F4/80, BM8; PerCP-eFluor710-CD115, AFS98 (eBioscience, San Diego, CA, USA); (2) for progenitor cells: FITC-CD117, 2B8 (eBioscience); PE-CD34, MEC14.7; PECy7-Ly6A/E, D7; BV-421-Lineage cocktail (Biolegend); Alexa Fluor 700-CD45, 30-F11 (BD Bioscience). Samples were washed once with FACS buffer, then with PBS, stained for 30 minutes, and placed on ice with APCefluor780-fixable/viability dye (eBioscience) for live/dead cell discrimination. After two more washes, cells were fixed with 1% formalin and acquired on a LSR Fortessa (BD Bioscience) flow cytometer (at the flow cytometry facility of Indiana University School of Medicine, Indianapolis, IN, USA). All cells (events) inside each tube were acquired for each sample to represent the total amount of cells per sample. CD45^{hi} and microglia cell numbers represent the total events acquired by flow cytometry in their respective gates of each sample. Data were analyzed using FlowJo 10.2 software (FlowJo, Ashland, OR, USA).

Varying DC of SRPT in GFP$^+$ Chimeric Mice

GFP BM reconstituted mice were subjected to SRPT in one eye using an infrared laser (Iridex OcuLight SLx MicroPulse 810

Investigative Ophthalmology & Visual Science

nm; IRIDEX, Mountain View, CA, USA) coupled to a slit-lamp. Variable DCs of 5%, 10%, 15%, and 20% ($n = 5$ animals each duty cycle) were used for 0.1 second at 250 mW and a spot size set to 50 μm. Thirty applications were administered to each eye circumferentially placed between 50 and 100 μm from the optic disc. An additional cohort of five WT age- and gender-matched animals did not receive SRPT, and those eyes were used as controls.

Two weeks later, eyes were harvested. The posterior segments were reacted with rabbit anti-cytokeratin (1:400; Dako A/S, Glostrup, Denmark), followed by an Alexa Fluor 488 goat anti-rabbit antibody (1:200; Abcam) used as the secondary. Slides were counterstained with DAPI. Posterior segments were mounted flat using four to five radial cuts and were then examined using an upright fluorescent microscope (DM2500; Leica). The area positive for eGFP was quantified using ImageJ software (http://imagej.nih.gov/ij/; provided in the public domain by the National Institutes of Health, Bethesda, MD, USA).

Adoptive Transfer of BM Stem Cells Following SRPT

Five WT mice were treated with 10% DC SRPT and then immediately given 15,000 cKit$^+$ Sca-1$^+$ BM cells from a GFP$^{+/+}$ donor via IV injection. Two weeks later the eyes were harvested, preserved, and cryosectioned. Sections were reacted with Alexa Fluor 488 goat anti-rabbit antibody, counterstained with DAPI, mounted, and examined as described.

Time Course and Tissue-Compartment Changes in Heat Shock Proteins (HSP), *Cxcl12*, and *Cxcr4* Involved in Cell Recruitment

To identify the possible mechanism for the SRPT-induced BM-derived cell recruitment to the NSR and RPE-choroid, we measured mRNA levels of HSP *Hspa1a* and *Hsp90aa1* and the known homing factor *Cxcl12* and its receptor *Cxcr4*. One eye ($n = 5$ per time point) of GFP chimeric mice was subjected to 10% DC SRPT. Mice were euthanized 2, 4, and 12 hours after SRPT application. Eyes from an additional cohort of five animals that did not receive SRPT served as controls. Eyes were dissected and the NSR and PC were separately homogenized in Trizol reagent (Invitrogen, Waltham, MA, USA), and RNA was isolated according to the manufacturer's instructions. First-strand cDNA was synthesized using SuperScript II reverse transcription (Invitrogen). Prepared cDNA was mixed with 2× SYBR Green PCR Master Mix (Applied Biosystems, Waltham, MA, USA) and appropriate gene-specific forward and reverse primers, then was subjected to real-time PCR quantification using the ABI PRISM 7700 Sequence Detection System (Applied Biosystems). All reactions were performed in triplicate. The relative amounts of mRNAs were calculated using the comparative threshold cycle method. All results were normalized to the abundance of *Actb*, which was used as endogenous control.

Time Course and Tissue-Compartment Changes in mRNA of Cytokines

The expression of inflammatory cytokines was examined in WT mice undergoing SRPT. For total RNA isolation, the RNeasy Mini Kit (Qiagen, Valencia, CA, USA) was used. One NSR and one RPE-choroid per sample were separately disrupted in 350 μL of lysis buffer with the TissueLyser LT (Qiagen) for 2 × 1 minute, using three to five 1-mm and twelve 3-mm zirconium oxide/yttria-stabilized beads (Union Process, Akron, OH, USA). The supernatants were further processed in a QIAcube (Qiagen) with the RNeasy Mini Kit. RNA quantity and quality was determined with NanoDrop 2000C (Thermo Scientific). For the reverse transcription, the SuperScript VILO cDNA Synthesis Kit (Thermo Scientific) was used according to manufacturer protocol, starting from 200 ng total RNA. For the PCR step, BioRad (Hercules, CA, USA) reagents were used as follows: primer sets for *Cryab*, *Hif1a*, *Tnfa*, *Il1b*, *Il6*, *Cxcl12*, *Ccl2*, and *Ifng*, and as endogenous control, *Actb*, as well as the SsoAdvanced Universal SYBR Green Supermix. The real-time PCR was performed in a ViiA7 Real-Time PCR System (Thermo Scientific) according to BioRad's suggested settings.

Statistical Analysis

Data were analyzed using GraphPad Prism 6.0 (GraphPad Software, La Jolla, CA, USA). One-way ANOVA was applied. Multiple comparisons were performed among all groups, with $P \leq 0.05$ considered significant.

Results

SRPT Does Not Disrupt the NSR or RPE Layer

The NSR and RPE layer were examined for evidence of damage following SRPT. As shown in Figure 1A–D, a time course study was performed in WT mice exposed to SRPT and euthanized at 12 hours, 24 hours, and 2 weeks following SRPT. No histologic evidence of NSR or RPE injury was observed in the experimental cohorts, and IBA$^+$ cells were observed in the NSR (Fig. 1).

Phenotypic and Time Course Characterization of the BM-Derived Cells That Home to the NSR and RPE

Characterization of the BM cells that homed to the retina was performed using flow cytometry. A significant increase in the total number of hematopoietic cells (CD45^{hi} cells) recruited to the NSR was observed 2 weeks following SRPT. The number of microglia was similarly increased at this time point (Fig. 2A). Temporal changes were observed in the content of infiltrating cells, especially at 24 hours post laser. A reduction of the percentage of lymphocytes was observed for T cells and other CD11b$^-$ cells and an increase in the percentage of monocytes (Fig. 2B), especially the inflammatory, Ly6C^{hi} cells (Fig. 2C). Neutrophil, dendritic cells, or macrophage percentages remained similar postlaser treatment.

In the RPE-choroid, we observed no significant increase in the total number of CD45^{hi} hematopoietic cells at any of the time points, and microglia were only increased at 2 weeks compared to 24 hours (Fig. 3A), although their abundance was very low compared to NSR. The composition of infiltrating CD45^{hi} in the RPE-choroid, in contrast to the NSR, changed significantly after laser treatment toward a more proinflammatory profile. As shown in Figure 3B, neutrophils were increased significantly within the first 24 hours, with a similar infiltration of monocytes. Among lymphocytes, T cells did not change significantly, but CD11b$^-$ cells were increased at 2 weeks; these cells could be B cells, natural killer cells, or progenitor cells, but not myeloid cells. Macrophages were increased at 2 weeks (Fig. 3B), indicating differentiation of infiltrating monocytes. The temporal increase in monocytes was in the Ly6C^{hi} population (Fig. 3C).

Because we observed an increase in CD11$^-$ cells in the RPE-choroid, we examined by flow cytometry the stem/progenitor cells recruited to the NSR and the RPE-choroid. In Figure 4, time-dependent changes are shown in the recruitment of progenitor cells, especially the Lin$^-$ Sca-1$^+$ (LS). In contrast, we

Investigative Ophthalmology & Visual Science

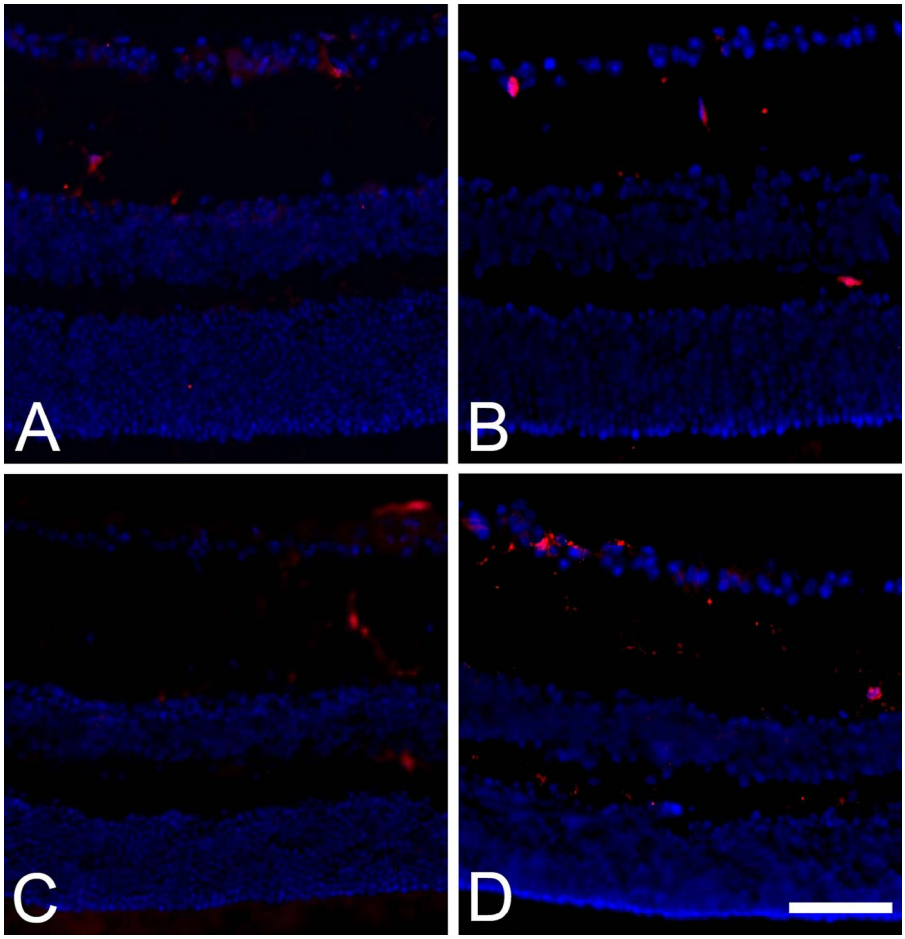

FIGURE 1. Subthreshold micropulse laser stimulates IBA-1$^+$ cell activation in the neural retina of WT mice in a time-dependent manner. (**A–D**) Representative images of frozen sections from eyes receiving 10% DC subthreshold micropulse laser and harvested at 0 (control, no laser) (**A**), 12 hours (**B**), 24 hours (**C**), and 2 weeks (**D**), respectively. *Scale bar*: In **D** = 40 μm and applies to all micrograph panels.

did not observe any recruitment of the Lin$^-$ c-kit$^+$ or the Lin$^-$ Sca-1$^+$ c-kit$^+$. LS cells were increased in the NSR, but not the RPE-choroid at 2 weeks post SRPT.

BM Cells Localization Following SRPT

Using GFP chimeric mice to more easily quantify the number of BM cells that home to the posterior cup, we next examined the impact of DC on the number and localization of GFP$^+$ cells. While a low number of GFP$^+$ cells were seen in the control chimeric animals, a robust recruitment of GFP$^+$ cells was observed in regions of laser-stimulated RPE 2 weeks following SRPT. We observed a DC-dependent homing of GFP$^+$ cells with a maximal response at 10% DC (Fig. 5A, B).

Using WT mice, we performed a short-term study. At time zero, there was no evidence of infiltration of BM-derived cells (Fig. 5C). However, 12 hours post SRPT, BM cells (Isolectin-B4 positive)[57–59] appeared to home to the RPE layer (Fig. 5D). Utilizing a second marker for BM cells, CD45, we observed and confirmed the association of BM cells with the RPE layer (Fig. 5E) at 12 hours post SRPT.

Exogenous BM Stem Cells Administered by Adoptive Transfer Localized to the RPE Layer

BM stem/progenitor cells can be isolated and introduced intravenously by a technique called adoptive transfer. WT mice received intravenous BM stem cells from GFP transgenic mice immediately after receiving 10% DC subthreshold micropulse laser. Eyes were harvested 2 weeks later and examined for expression of GFP. GFP cells were found that homed to and localized to the RPE layer (Fig. 6).

Micropulse Laser Induces a Time- and Tissue Compartment–Dependent Change in mRNA Expression of Key Protective Proteins and Molecular Chaperones

To identify the possible mechanism for the micropulse laser–induced BM-derived cell recruitment to the retina, we measured the time course of mRNA levels of the *Hspa1a* and *Hsp90aa1* and *Cryab*, after using a diode laser (810 nM) and 10% DC. A peak increase in *Hspa1a* was observed 2 hours post laser in the NSR and at 4 hours in RPE-choroid (Fig. 7A). At 2 hours, mRNA for *Hsp90aa1* dramatically peaked in both the NSR and the RPE-choroid (Fig. 7B). *Cryab* showed a marked increase at 2 hours in the NSR but a decrease at 12 hours in the NSR. In contrast, the levels of *Cryab* in the RPE-choroid showed a decrease at 2 and 4 hours (Fig. 7C).

Following SRPT, we observed that *Hif1a* mRNA (Fig. 7D) was reduced at 2 hours in both the NSR and the RPE-choroid, but increased above baseline in the RPE-choroid at 4 hours. Since the BM cell homing factor, CXCL-12 (or stromal-derived

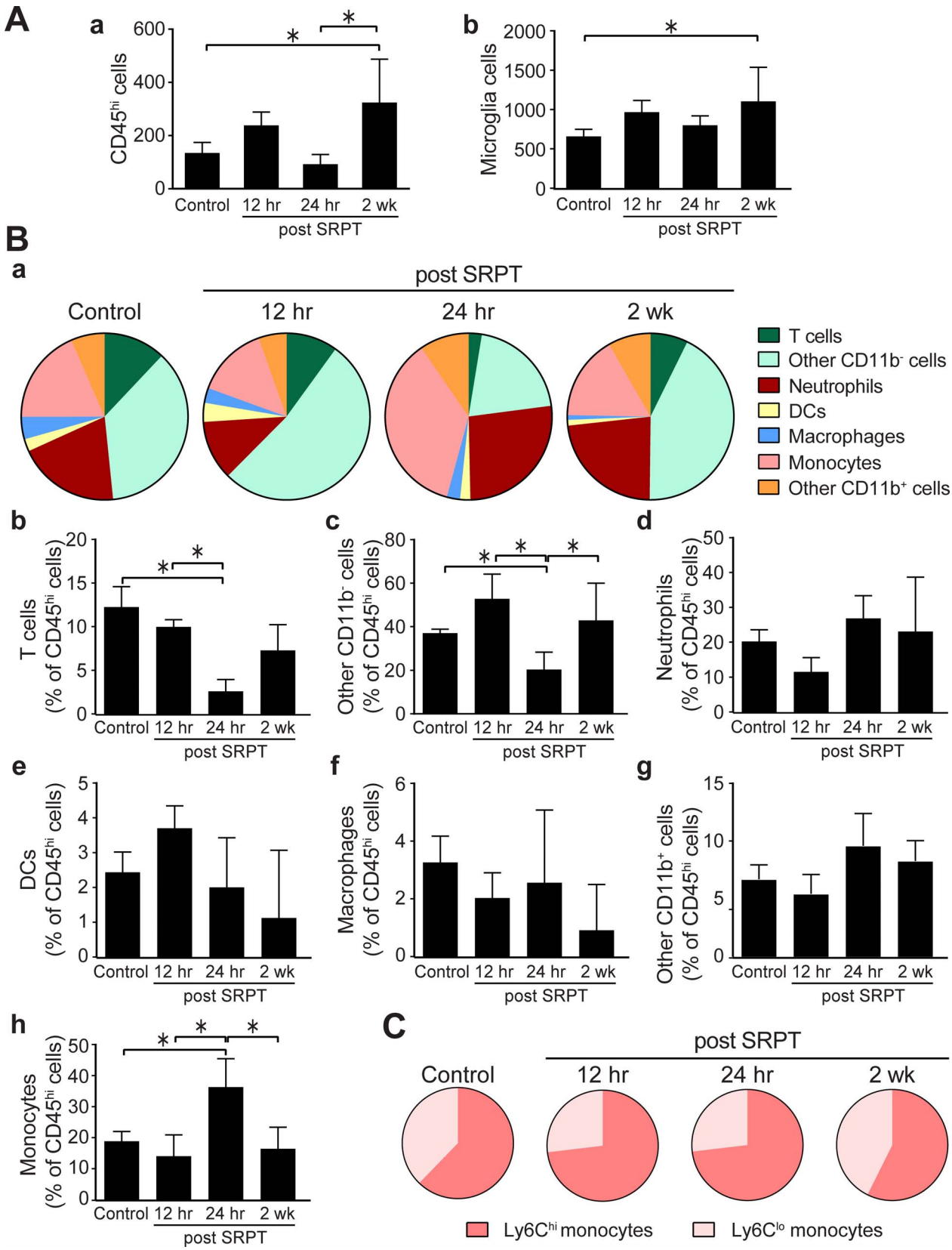

Figure 2. Time-dependent changes in the recruitment of BM-derived $CD45^{hi}$ cells in the NSR. Mouse eyes were subjected to 10% DC subthreshold micropulse laser. Eyes were harvested and retinas were prepared for flow cytometry. (**A**) Percentages of $CD45^{hi}$ and microglia ($CD45^{lo}$ $F480^{hi}$ cells in the retina; means ± SD, $n = 4$–7 per time point). (**B**) The composition of $CD45^{hi}$ cell recruitment in the retina after STPT. *Bar graphs* represent the means ± SD for each subset of cells ($^*P < 0.05$, 1-way ANOVA). (**C**) The composition of monocytes as $Ly6C^{hi}$ and $Ly6C^{lo}$ subsets after STPT.

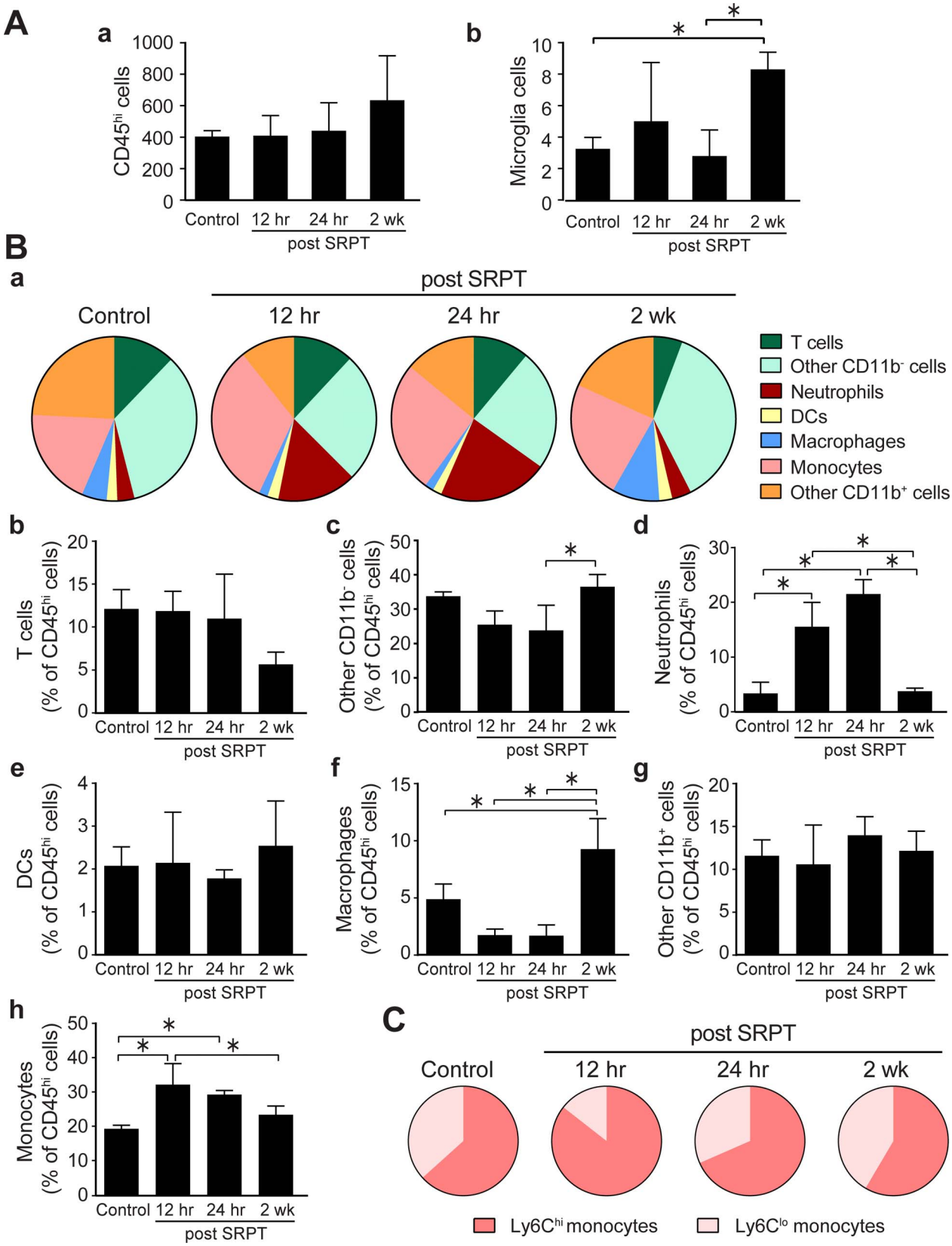

Figure 3. Time-dependent changes in the recruitment of BM-derived CD45^{hi} cells in the RPE-choroid. Mouse eyes were subjected to 10% DC subthreshold micropulse laser and harvested at times indicated. Eyes were dissected and RPE-choroid was prepared for flow cytometry. (**A**) Percentages of CD45^{hi} and microglia (CD45^{lo} F480^{hi} cells in the RPE layer; means ± SD, $n = 4$–7 per time point). (**B**) The composition of CD45^{hi} cell recruitment to the RPE layer after STPT. *Bar graphs* represent the means ± SD for each subset of cells (*$P < 0.05$, 1-way ANOVA). (**C**) The composition of monocytes as Ly6C^{hi} and Ly6C^{lo} subsets after STPT.

Investigative Ophthalmology & Visual Science

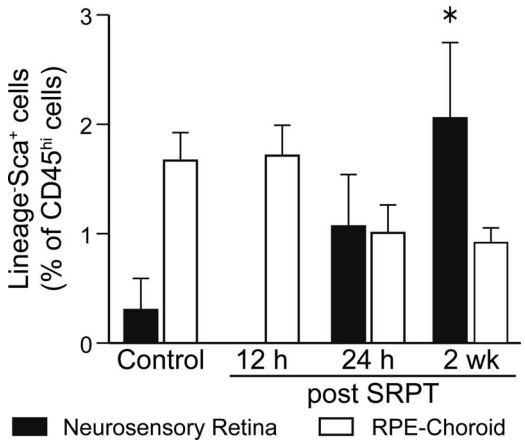

Figure 4. Time-dependent changes in the recruitment of BM Lineage$^-$ Sca$^+$ progenitor cells in the NSR and the RPE-choroid. Mouse eyes were subjected to 10% DC subthreshold micropulse laser, eyes were harvested, and the NSRs or RPE-choroids were prepared for flow cytometry. Percentages of LS cells ($^*P < 0.05$, 1-way ANOVA for each tissue).

factor-1 [SDF-1]), and its receptor CXCR-4 are similarly hypoxia regulated, we next examined mRNA expression for *Cxcl12* and *Cxcr4*. Within 2 hours of laser treatment, expression of *Cxcl12* (Fig. 7E) and its receptor *Cxcr4* (Fig. 7F) decreased in the NSR and RPE-choroid. *Cxcl12* mRNA increased at 4 hours in the RPE-choroid. However, by 4 hours post laser, *Cxcr4* returned to normal baseline levels in NSR but was increased in the RPE-choroid at 12 hours.

Micropulse Laser Induces a Time- and Tissue Compartment–Dependent Change in mRNA Expression of Key Cytokines

We next performed an extended time course of 12 hours to 2 weeks, and we observed an increase in *Ccl2* mRNA in the RPE-choroid but not in the NSR. *Cxcr4* mRNA expression was observed in the RPE-choroid at 24 hours. *Il1b* mRNA increased in the RPE-choroid at 12 and 24 hours. *IL6* mRNA increased in the RPE-choroid but not the NSR at 12 hours. *Ifng* mRNA decreased at 12 hours and then increased at 24 hours in the RPE-choroid. *Tnfa* mRNA did not change over time following SRPT (Fig. 8).

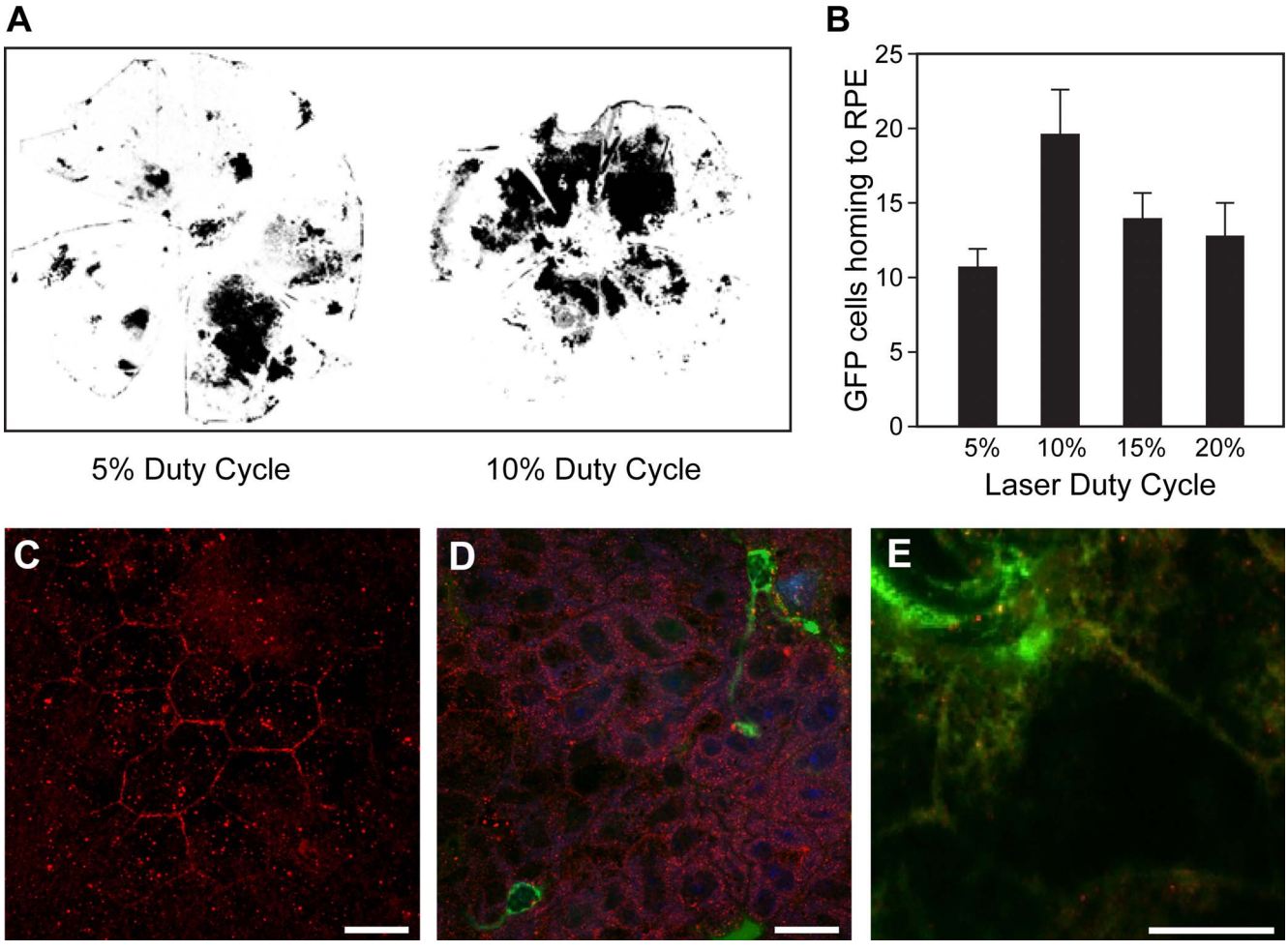

Figure 5. Subthreshold micropulse laser stimulates BM cells to migrate to RPE layer of affected eyes of GFP$^+$ chimeric mice. (**A**) Representative binary images of flat-mounted posterior cups (neural retina removed) imaged under epifluorescence to detect GFP show the patterns of homing to areas subjected to laser application in chimeric mice 14 days following SRPT. (**B**) Quantification of the area positive for eGFP shows a 10% DC is sufficient for maximal effect. $^*P < 0.05$ vs. 5% duty cycle; $n = 5$ for each condition. (**C**) A continuous layer of RPE cells (Occludin-positive, *red*) without evidence of BM cells at time zero. (**D**) Evidence of IB-4$^+$ cells (*green*) associated with RPE cells (Occludin-positive, *red*) following SRPT at 12-hour time point. (**E**) CD45$^+$ cells (*green*) associated with RPE cells at higher magnification at the 12-hour time point. *Scale bars*: 10 μm.

Investigative Ophthalmology & Visual Science

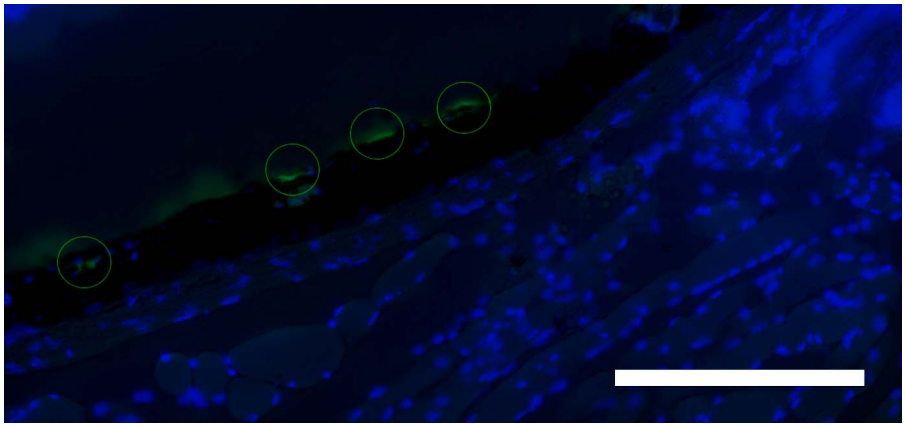

FIGURE 6. Adoptive transfer of BM stem cells following SRPT results in localization to the RPE layer. Eyes from WT mice that received intravenous BM stem cells from $GFP^{+/+}$ transgenic mice immediately after 10% DC subthreshold micropulse laser and harvested 14 days later were cryosectioned. GFP BM cells associated with RPE layer. The representative captured images shown are a merge of bright field and *green* (GFP) and *blue* (DAPI) channels. *Scale bar*: 25 μm.

DISCUSSION

The salient finding of this study is the demonstration, we believe for the first time, that BM-derived cells can be locally recruited to the retina, including the RPE layer, using SRPT. We did not observe any histologic evidence of damage in the NSR or RPE-choroid (Fig. 1). Using flow cytometry, we determined that the primary cell type that responded early (within 24 hours) to SRPT were monocytes (primarily $Ly6C^{hi}$) and other $CD11b^{-}$ cells, whereas microglia cells ($IBA\text{-}1^{+}$ cells) increased at 2 weeks. The early inflammatory cells reestablished their homeostatic levels by 2 weeks, but microglia number increased. In the RPE-choroid, neutrophils and monocytes ($Ly6C^{hi}$) were increased at the early time points, whereas macrophages and microglial cells were increased at the later time point of 2 weeks. These results are in keeping with our observed increase in GFP^{+} cell localization to the RPE layer observed in GFP chimeric mice and in the adoptive transfer studies.

We also found that SRPT primed the RPE-choroid, resulting in an increase in the expression for the molecular chaperones *Hspa1a*, *Hsp90aa1*, and the small HSP. *Cryab* mRNA expression and subsequently an increase in *Hif1a*, *Cxcl12I*, and *Cxcr4* mRNA was observed. Moreover, unlike the CW laser, SRPT was inherently nondestructive. The stimulation to the NSR and RPE-choroid could be considered as photochemical in nature, with the resultant increase in mRNA for key reparative proteins serving to protect the retina and RPE and signal recruitment of BM-derived cells to the retina. While the precise cascade of events remains unknown, we have observed unique temporal events. This photochemical stimulation[52–56] likely induced mild oxidative stress, stimulating recruitment of BM-derived microglia.[60,61] Oxidative injury launches the necessary inflammatory pathways, including microglial activation to foster tissue repair.[62] We also observed an induction of *Hif1a* mRNA possibly due to laser-induced local hypoxia, which in turn is followed by the increase in expression of hypoxia-regulated *Cxcl12* and *Cxcr4* mRNAs. These events, we postulate, set the stage for the next round of repair (and next round of BM-derived cell recruitment). Two weeks post SRPT, BM marrow-derived cells specifically home to the RPE-choroid.[63] The ultimate fate of the BM cells remains unclear as the current study represents a short (2-week) time course.

In the current study, we focused on the 10% DC, chosen because at this DC BM-derived cell mobilization to the RPE was maximal. This raises the possibility of a therapeutic "sweet spot" in terms of future clinical applications. Micropulse laser using a 5% DC has been demonstrated to be efficacious in the treatment of DME.[64,65] If there is a BM-derived stem cell contribution to resolution of macular edema following mircopulse laser, then perhaps a potentially greater benefit may be observed if the 10% DC is employed rather than the current 5%. Ultimately, this 10% vs. 5% DC therapeutic quandary would require investigation within a clinical trial framework because the current rodent model may not accurately reflect the response of a diabetic macula to micropulse laser. BM-derived reparative cells that home to the retina and RPE likely promote their beneficial effect by their paracrine production of growth factors and cytokines, including those that can potentially reduce DME.[66]

The HSP response to photochemical stress was not unexpected.[52–56,67] Although there was no damage evident to the NSR histologically, increased expression of these proteins and $IBA\text{-}1^{+}$ cell recruitment suggest the possibility of some photochemical damage of the NSR overlying the RPE treatment zone.[52–56] It is also interesting to speculate that HSPs and CXCL-12 may play a role in the resolution of DME following micropulse laser therapy.[38,64,65,67] Whereas the mRNA expression of *Hspa1a* and *Hsp90aa1* in the NSR and the RPE-choroid tended to mirror each other, *Cryab* (α-crystallin B) mRNA showed a marked increase at 2 hours in the NSR but a decrease at each time point in the RPE. This observation may signify that initially SRPT may shock or stun the RPE, an effect that is reflected in the initial decrease in α-crystallin B expression before recovery back toward baseline levels. Alternatively, because α-crystallin B in some situations can be a negative regulator of inflammation, in an acute situation such as the laser model described herein, a temporary downregulation of this small HSP may be essential to promote the acute physiologic inflammatory response in the retina[68–70] that we observed as microglia recruitment.

The acute reparative response we observed in our model is in sharp contrast to the chronic inflammatory environment that is the pathologic hallmark of both AMD and DR.[71,72] In these latter scenarios, the microglial response is inappropriate, representing chronic activation, and is likely responsible for upregulation of proinflammatory cytokines. Thus, our studies support that the acute/physiologic versus chronic/pathologic microglia activation is a key factor in determining the behavior and fate of these cells and their role in disease. In the study by Chidlow et al.,[71] CW laser was compared with nonthermal nanopulse laser in a rat model. They demonstrated colocaliza-

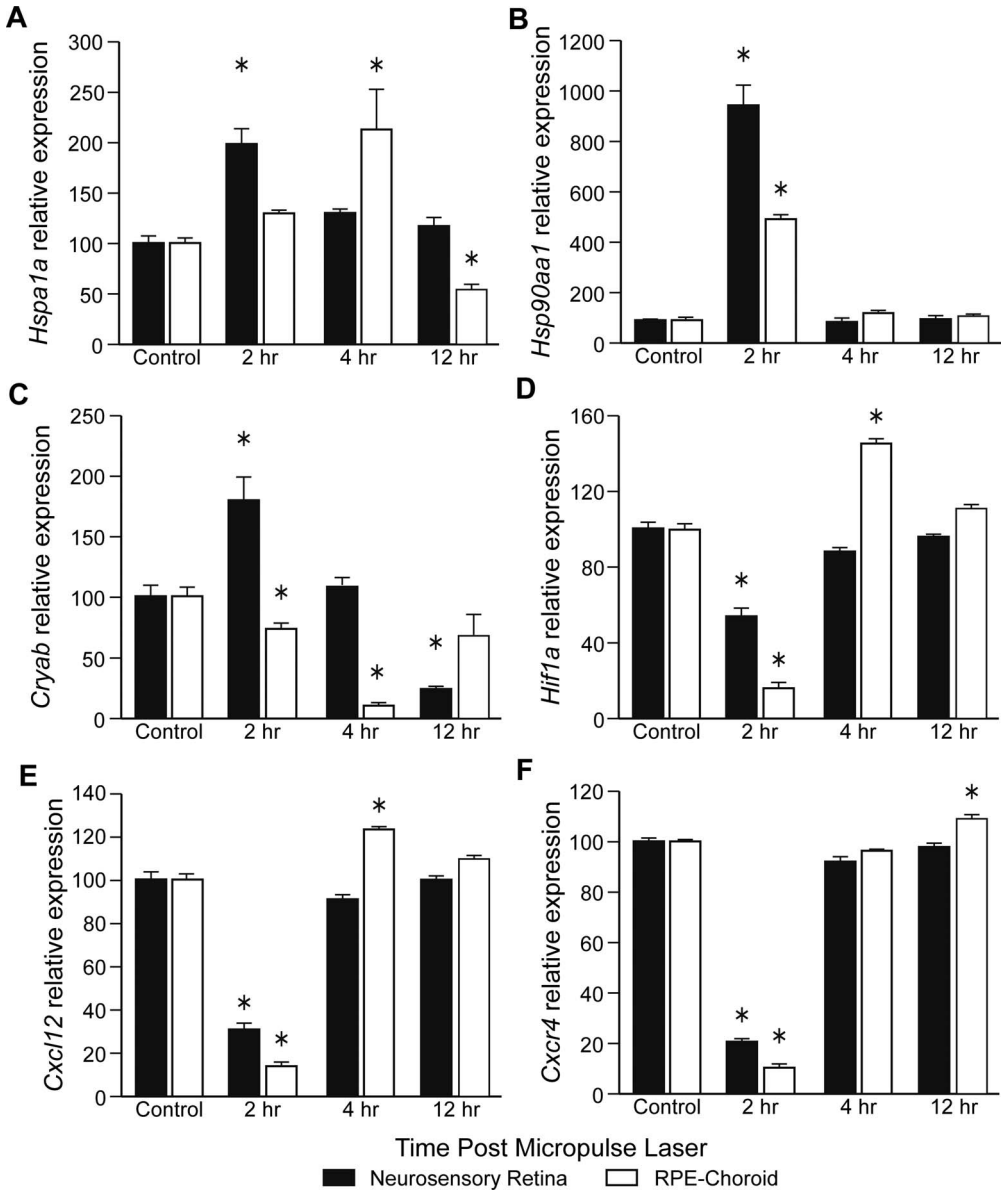

Figure 7. Time- and tissue compartment–dependent changes in mRNA expression of proteins involved in cell recruitment in GFP chimeric mice. Mouse eyes were subjected to 10% DC subthreshold micropulse laser and harvested at the indicated time points. Eyes were dissected, mRNA was extracted separately from NSR and RPE-choroid, and real-time PCR quantification was performed. All reactions were performed in triplicate. The relative amounts of mRNAs were calculated using the $2^{-\Delta\Delta Cq}$ method, using *Actb* as endogenous control. (**A**) *Hsp1a1*. (**B**) *Hsp90aa1*. (**C**) *Cryab*. (**D**) *Hif1a*. (**E**) *Cxcl12*. (**F**) *Cxcr4*. Data are means ± SEM; $^*P < 0.05$ versus control, $n = 5$ mice per time point.

tion of the inflammatory cytokines IL-1β and TNF-α with microglia in both laser modes, with peak levels being observed at the 6-hour time point.[71] The nature of the IBA-1$^+$ response is likely dependent on the nature of the laser injury.[73] A severe laser injury may activate a pathologic microglial response, defined as an exuberant acute inflammatory response characterized by significant and prolonged microglial migration to the outer segments and activation in the presence of excessive proinflammatory cytokines. This would lead to destruction of local tissue and/or excessive recruitment and deposition of scar tissue. A less severe injury, such as one resulting from micro- or nanopulse laser would likely induce an acute inflammatory response that is self-modulating and self-limiting, in that tissue repair will be complete and lead to normal return of function and cellular homeostasis. Jobling et al.,[74] in their study to determine the effect of nanopulse laser in subjects with bilateral intermediate AMD, proposed that one of the possible mechanisms whereby nanopulse laser may be beneficial was that there was no activation of the microglia in the NSR.[74] The implication is that microglial activation could generate an exuberant and prolonged inflammatory response similar to AMD and therefore promote progression of disease.[74,75]

Inagaki et al.[76] investigated the effects of sublethal laser energy using an in vitro model where photocoagulation-like areas were created in cultured ARPE-19 cell layers.[76] Hsp70 mRNA expression was induced within 30 minutes of laser irradiation, peaking at 3 hours after irradiation, which was dependent on the number of laser pulses. Hsp70 protein expression occurred concentrically around laser irradiation sites and persisted for 24 hours following irradiation. They concluded that sublethal photothermal stimulation with a

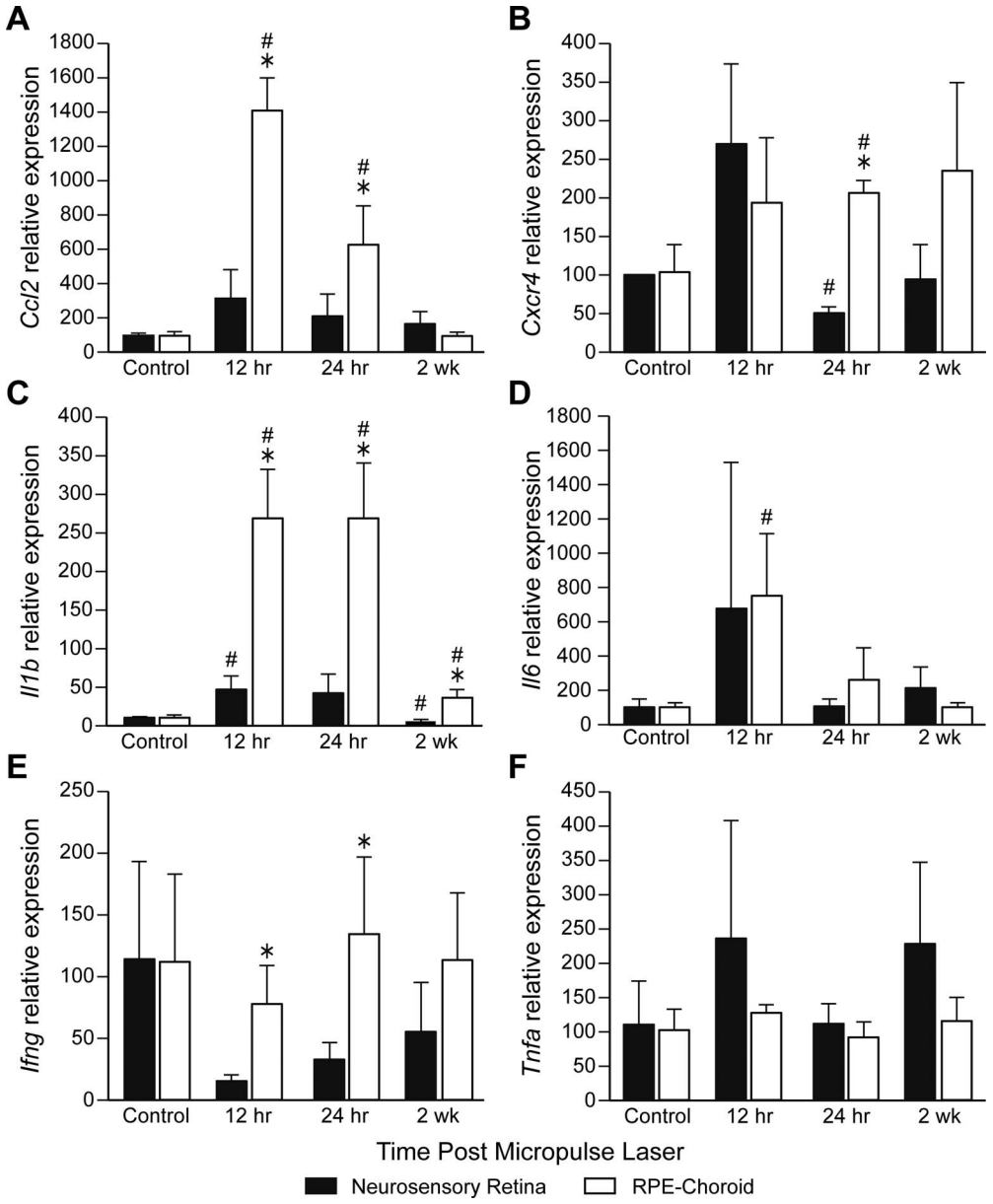

Figure 8. Time- and tissue compartment–dependent changes in mRNA expression of key cytokines in WT mice. Mouse eyes were subjected to 10% DC subthreshold micropulse laser and harvested at indicated time points. Eyes were dissected, mRNA was extracted separately from NSR and RPE-choroid, and real-time PCR quantification was performed. All reactions were performed in duplicate. The relative amounts of mRNAs were calculated using the $2^{-\Delta\Delta Cq}$ method, using *Actb* as endogenous control. (**A**) *Cxcl2*. (**B**) *Cxcr4*. (**C**) *Il1b*. (**D**) *Il6*. (**E**) *Ifng*. (**F**) *Tnfa*. Data are means ± SEM; $^{\#}P < 0.05$ versus control; $^{*}P < 0.05$ between NSR and RPE-choroid; $n = 5$ mice per time point.

micropulse laser may facilitate Hsp70 expression in the RPE without inducing cellular damage.[76]

Based on the observations of the current study and those of Jobling et al.,[74] we can propose the concept of a laser-induced therapeutic or inflammatory threshold. With a low-dose pulse laser, the induced inflammatory response is below an acute inflammatory threshold that gives rise to injury; it rather represents a tempered physiological response. Whereas with CW laser, regardless of whether it is visible or subvisible, the inflammatory response is greater than the threshold, a process that leads to inevitable destruction of the NSR, which may be accompanied by excessive microglial activation.

Nanopulse laser therapy has also demonstrated benefits in both the treated and untreated eyes with nonexudative AMD.[74,77] When one considers that the current study demonstrated mobilization of BM-derived cells and therefore the potential for a systemic (and potentially) therapeutic contribution to a local disease, then perhaps regression of drusen and improvement in central retinal flicker threshold in the fellow eye are not surprising findings from these studies, as these cells would be expected to home to any site where disease is present. Furthermore, it raises the tantalizing specter of laser-guided mobilization and homing of BM-derived cells as a viable therapeutic option in the management of disease, as well as an option to guide stem cells following systemic

adoptive transfer, as we show. We recently showed that BM-derived cells can be administered systemically and are directed to the RPE layer where they integrate into the damaged RPE, fostering repair.[78]

It is reasonable to envisage micropulse laser as more than just a one-time therapy in that it should be possible to repeat treatment when indicated. Furthermore, micropulse laser does not have the side effects associated with CW laser.[30,34–41] Our results suggest that the therapeutic effect of micropulse involves a systemic component, in addition to locally induced effects. Although the precise mechanism of action of SRPT remains unknown, the current study provides evidence that it involves mobilization and recruitment of BM cells.

Although DME is part of a retinopathy that mainly involves the inner blood retinal barrier, the beneficial effects of laser that targets the RPE are long established.[28–30,38] Despite this, the precise mechanism of action of laser remains elusive.[42–51] However, the limitations of this study must be acknowledged as this laser model is neither a model of disease nor may it accurately reflect the human retina. Increased expression of α-crystallin B has been reported elsewhere to be essential for the maintenance of vascular integrity in the retina via its modulatory effects on VEGF function.[79] Our studies would also support laser-induced rejuvenation of microglia responding to CXCL-12 gradients as a potential contributor to the beneficial mechanism of action.[80] Micro- or nanopulse therapy activates a tissue repair response.[62]

In the initial stages of micro- or nanopulse therapy, an appropriate response (upregulation of HSPs, HIF1-α, and CXCL-12, as well as infiltration of systemic immune cells, including BM-derived cells) sets in motion the necessary train of events to elicit repair. This response could repair macular edema resulting from breakdown of the inner blood retinal barrier or promote resolution of drusen and remodeling of Bruch's membrane in nonexudative AMD.[38,67,71,72,74,81] With the potential tissue benefits of SRPT as outlined here, this form of laser may have benefits beyond the currently recognized treatment of DME.[30,64,82,83]

Micropulse laser therapy can also be considered for the treatment of macular edema occurring secondary to central and branch retinal vein occlusion and even in the treatment of, and as a possible alternative to, panretinal photocoagulation for the treatment of proliferative retinopathies.[84] In this latter situation, SRPT, through augmentation of BM cells and the association of the latter with the maintenance of vascular integrity, may have a sufficient therapeutic benefit that does not require photocoagulation of retinal tissue and instead promotes repair.[67] In addition, micropulse phototherapy promotes resensitization of the retina to intravitreal anti-VEGF therapy in individuals who have become refractory to this treatment.[85] This further begs the question whether this beneficial action on the retina is all or in part due to BM cell recruitment. Finally, and perhaps most importantly, and similar to the observed benefits of nanopulse therapy in the treatment of intermediate AMD, SRPT could provide an alternative treatment modality that retards, arrests, or even rejuvenates the retina without inducing retinal damage, even when used unilaterally.[74,77] This would be an era-defining breakthrough in the treatment of nonexudative AMD, for which there is currently no effective treatment. Elderly patients who are afflicted with AMD typically have reduced levels of reparative BM-derived $CD34^+$ cells in their circulation.[86–88] The use of SRPT may facilitate the release of BM-derived cells into the circulation followed by their homing to the site of laser stimulation in the retina for the repair and maintenance of the RPE, consequently promoting improved turnover of Bruch's membrane by the RPE. Investigation of SRPT in these various clinical scenarios would require formal clinical trials.

Acknowledgments

The authors thank the Flow Cytometry Resource Facility at Indiana University Simon Cancer Center (partially funded by National Cancer Institute Grant P30 CA082709).

Supported by National Institutes of Health Grants HL110170, EY023629, EY012601, and EY007739 (to MBG).

Disclosure: **S. Caballero**, None; **D.L. Kent**, None; **N. Sengupta**, None; **S. Li Calzi**, None; **L. Shaw**, None; **E. Beli**, None; **L. Moldovan**, None; **J.M. Dominguez II**, None; **R.S. Moorthy**, None; **M.B. Grant**, None

References

1. Age-Related Eye Disease Study Research Group. A randomized, placebo-controlled, clinical trial of high-dose supplementation with vitamins C and E, beta carotene, and zinc for age-related macular degeneration and vision loss: AREDS report no. 8. *Arch Ophthal*. 2001;119:1417–1436.
2. Age-Related Eye Disease Study 2 Research Group. Lutein + zeaxanthin and omega-3 fatty acids for age-related macular degeneration: the Age-Related Eye Disease Study 2 (AREDS2) randomized clinical trial. *JAMA*. 2013;309:2005–2015.
3. Kiewisz J, Kaczmarek MM, Pawlowska A, Kmiec Z, Stompor T. Endothelial progenitor cells participation in cardiovascular and kidney diseases: a systematic review. *Acta Biochim Pol*. 2016;63:475–482.
4. Faiella W, Atoui R. Therapeutic use of stem cells for cardiovascular disease. *Clin Transl Med*. 2016;5:34.
5. Moisseiev E, Smit-McBride Z, Oltjen S, et al. Intravitreal administration of human bone marrow CD34+ stem cells in a murine model of retinal degeneration. *Invest Ophthalmol Vis Sci*. 2016;57:4125–4135.
6. Caballero S, Hazra S, Bhatwadekar A, et al. Circulating mononuclear progenitor cells: differential roles for subpopulations in repair of retinal vascular injury. *Invest Ophthalmol Vis Sci*. 2013;54:3000–3009.
7. Chan-Ling T, Baxter L, Afzal A, et al. Hematopoietic stem cells provide repair functions after laser-induced Bruch's membrane rupture model of choroidal neovascularization. *Am J Pathol*. 2006;168:1031–1044.
8. Harris JR, Brown GA, Jorgensen M, et al. Bone marrow-derived cells home to and regenerate retinal pigment epithelium after injury. *Invest Ophthalmol Vis. Sci*. 2006;47:2108–2113.
9. Grant MB, May WS, Caballero S, et al. Adult hematopoietic stem cells provide functional hemangioblast activity during retinal neovascularization. *Nat Med*. 2002;8:607–612.
10. Sengupta N, Caballero S, Sullivan SM, et al. Regulation of adult hematopoietic stem cells fate for enhanced tissue-specific repair. *Molecular Ther*. 2009;17:1594–1604.
11. Park SS, Bauer G, Abedi M, et al. Intravitreal autologous bone marrow CD34+ cell therapy for ischemic and degenerative retinal disorders: preliminary phase 1 clinical trial findings. *Invest Ophthalmol Vis Sci*. 2015;56:81–89.
12. Sharma A, Gokulchandran N, Chopra G, et al. Administration of autologous bone marrow-derived mononuclear cells in children with incurable neurological disorders and injury is safe and improves their quality of life. *Cell Transplant* 2012;21(suppl 1):S79–S90.
13. Yamout B, Hourani R, Salti H, et al. Bone marrow mesenchymal stem cell transplantation in patients with multiple sclerosis: a pilot study. *J Neuroimmunol*. 2010;227:185–189.
14. Sanberg PR, Park DH, Kuzmin-Nichols N, et al. Monocyte transplantation for neural and cardiovascular ischemia repair. *J Cell Mol Med*. 2010;14:553–563.

15. Gnecchi M, Zhang Z, Ni A, Dzau VJ. Paracrine mechanisms in adult stem cell signaling and therapy. *Circ Res*. 2008;103: 1204–1219.
16. Iekushi K, Seeger F, Assmus B, Zeiher AM, Dimmeler S. Regulation of cardiac microRNAs by bone marrow mononuclear cell therapy in myocardial infarction. *Circulation*. 2012; 125:1765–1773.
17. Cook LL, Persinger MA. Infiltration of lymphocytes in the limbic brain following stimulation of subclinical cellular immunity and low dosages of lithium and a cholinergic agent. *Toxicol Lett*. 1999;109:77–85.
18. Longo B, Romariz S, Blanco MM, et al. Distribution and proliferation of bone marrow cells in the brain after pilocarpine-induced status epilepticus in mice. *Epilepsia*. 2010;51:1628–1632.
19. Chakravarthy H, Beli E, Navitskaya S, et al. Imbalances in mobilization and activation of pro-inflammatory and vascular reparative bone marrow-derived cells in diabetic retinopathy. *PLoS One*. 2016;11:e0146829.
20. Schilling M, Besselmann M, Leonhard C, Mueller M, Ringelstein EB, Kiefer R. Microglial activation precedes and predominates over macrophage infiltration in transient focal cerebral ischemia: a study in green fluorescent protein transgenic bone marrow chimeric mice. *Exp Neurol*. 2003; 183:25–33.
21. Vallieres L, Sawchenko PE. Bone marrow-derived cells that populate the adult mouse brain preserve their hematopoietic identity. *J Neurosci*. 2003;23:5197–5207.
22. Bernardino L, Ferreira R, Cristovao AJ, Sales F, Malva JO. Inflammation and neurogenesis in temporal lobe epilepsy. *Curr Drug Targets CNS Neurol Disord*. 2005;4:349–360.
23. Ginhoux F, Lim S, Hoeffel G, Low D, Huber T. Origin and differentiation of microglia. *Front Cell Neurosci*. 2013;7:45.
24. Beli E, Dominguez JM II, Hu P, et al. CX3CR1 deficiency accelerates the development of retinopathy in a rodent model of type 1 diabetes. *J Mol Med (Berl)*. 2016;94:1255–1265.
25. Chakravarthy H, Navitskaya S, O'Reilly S, et al. Role of acid sphingomyelinase in shifting the balance between proinflammatory and reparative bone marrow cells in diabetic retinopathy. *Stem Cells*. 2016;34:972–983.
26. Hu P, Thinschmidt JS, Caballero S, et al. Loss of survival factors and activation of inflammatory cascades in brain sympathetic centers in type 1 diabetic mice. *Am J Physiol Endocrinol Metab*. 2015;308:E688–E698.
27. Hu P, Thinschmidt JS, Yan Y, et al. CNS inflammation and bone marrow neuropathy in type 1 diabetes. *Am J Pathol*. 2013; 183:1608–1620.
28. Early Treatment Diabetic Retinopathy Study Research Group. Photocoagulation for diabetic macular edema: early treatment diabetic retinopathy study report number 1. *Arch Ophthalmol*. 1985;103:1796–1806.
29. Early Treatment Diabetic Retinopathy Study Research Group. Photocoagulation for diabetic macular edema: early treatment diabetic retinopathy study report number 4. *Int Ophthalmol Clin*. 1987;27:265–272.
30. Akduman L, Olk RJ. Laser photocoagulation of diabetic macular edema. *Ophthalmic surgery and lasers*. 1997;28: 387–408.
31. Macular Photocoagulation Study Group. Argon laser photocoagulation for senile macular degeneration. Results of a randomized clinical trial. *Arch Ophthalmol*. 1982;100:912–918.
32. The Branch Vein Occlusion Study Group. Argon laser photocoagulation for macular edema in branch vein occlusion. *Am J Ophthalmol*. 1984;98:271–282.
33. Olk RJ. Modified grid argon (blue-green) laser photocoagulation for diffuse diabetic macular edema. *Ophthalmology*. 1986;93:938–950.
34. Guyer DR, D'Amico DJ, Smith CW. Subretinal fibrosis after laser photocoagulation for diabetic macular edema. *Am J Ophthalmol*. 1992;113:652–656.
35. Hudson C, Flanagan JG, Turner GS, Chen HC, Young LB, McLeod D. Influence of laser photocoagulation for clinically significant diabetic macular oedema (DMO) on short-wavelength and conventional automated perimetry. *Diabetologia*. 1998;41:1283–1292.
36. Lewis H, Schachat AP, Haimann MH, et al. Choroidal neovascularization after laser photocoagulation for diabetic macular edema. *Ophthalmology*. 1990;97:503–510; discussion 510–501.
37. Schatz H, Madeira D, McDonald HR, Johnson RN. Progressive enlargement of laser scars following grid laser photocoagulation for diffuse diabetic macular edema. *Arch Ophthalmol*. 1991;109:1549–1551.
38. Dorin G. Evolution of retinal laser therapy: minimum intensity photocoagulation (MIP). Can the laser heal the retina without harming it? *Semin Ophthalmol*. 2004;19:62–68.
39. Luttrull JK, Dorin G. Subthreshold diode micropulse laser photocoagulation (SDM) as invisible retinal phototherapy for diabetic macular edema: a review. *Curr Diabetes Rev* 2012;8: 274–284.
40. Marshall J. Thermal and mechanical mechanisms in laser damage to the retina. *Invest Ophthalmol*. 1970;9:97–115.
41. Paulus YM, Jain A, Gariano RF, et al. Healing of retinal photocoagulation lesions. *Invest Ophthalmol Vis Sci*. 2008; 49:5540–5545.
42. Budzynski E, Smith JH, Bryar P, Birol G, Linsenmeier RA. Effects of photocoagulation on intraretinal PO2 in cat. *Invest Ophthalmol Vis Sci*. 2008;49:380–389.
43. Foulds WS, Kaur C, Luu CD, Kek WK. A role for photoreceptors in retinal oedema and angiogenesis: an additional explanation for laser treatment? *Eye*. 2010;24:918–926.
44. Foulds WS, Moseley H, Eadie A, McNaught E. Vitreal, retinal, and pigment epithelial contribution to the posterior blood-ocular barrier. *Trans Ophthalmol Soc U K*. 1980;100:341–342.
45. Gottfredsdottir MS, Stefansson E, Jonasson F, Gislason I. Retinal vasoconstriction after laser treatment for diabetic macular edema. *Am J Ophthalmol*. 1993;115:64–67.
46. Landers MB III, Stefansson E, Wolbarsht ML. Panretinal photocoagulation and retinal oxygenation. *Retina*. 1982;2: 167–175.
47. Molnar I, Poitry S, Tsacopoulos M, Gilodi N, Leuenberger PM. Effect of laser photocoagulation on oxygenation of the retina in miniature pigs. *Invest Ophthalmol Vis Sci*. 1985;26:1410–1414.
48. Pournaras CJ, Tsacopoulos M, Strommer K, Gilodi N, Leuenberger PM. Scatter photocoagulation restores tissue hypoxia in experimental vasoproliferative microangiopathy in miniature pigs. *Ophthalmology*. 1990;97:1329–1333.
49. Stefansson E. Oxygen and diabetic eye disease. *Albrecht von Graefes Archiv fur klinische und experimentelle Ophthalmologie* 1990;228:120–123.
50. Stefansson E, Hatchell DL, Fisher BL, Sutherland FS, Machemer R. Panretinal photocoagulation and retinal oxygenation in normal and diabetic cats. *Am J Ophthalmol*. 1986;101:657–664.
51. Stefansson E, Machemer R, de Juan E Jr, McCuen BW II, Peterson J. Retinal oxygenation and laser treatment in patients with diabetic retinopathy. *Am J Ophthalmol*. 1992;113:36–38.
52. Mainster MA. Solar retinitis, photic maculopathy and the pseudophakic eye. *J Am Intraocul Implant Soc*. 1978;4:84–86.

Investigative Ophthalmology & Visual Science

53. Mainster MA. Light and macular degeneration: a biophysical and clinical perspective. *Eye*. 1987;1(Pt 2):304–310.
54. Mainster MA, Ham WT Jr, Delori FC. Potential retinal hazards. Instrument and environmental light sources. *Ophthalmology*. 1983;90:927–932.
55. Rozanowska M, Handzel K, Boulton ME, Rozanowski B. Cytotoxicity of all-trans-retinal increases upon photodegradation. *Photochem Photobiol*. 2012;88:1362–1372.
56. Whitacre MM, Manoukian N, Mainster MA. Argon indirect ophthalmoscopic photocoagulation: reduced potential phototoxicity with a fixed safety filter. *Br J Ophthalmol*. 1990;74: 233–234.
57. Iwatsuki H, Sasaki K, Suda M, Itano C. Origin of the central cells of erythroblastic islands in fetal mouse liver: ultrahistochemical studies of membrane-bound glycoconjugates. *Histochem Cell Biol*. 1997;107:459–468.
58. Medana IM, Hunt NH, Chan-Ling T. Early activation of microglia in the pathogenesis of fatal murine cerebral malaria. *Glia*. 1997;19:91–103.
59. Kuemmel TA, Thiele J, Hafenrichter EG, Varus E, Fischer R. Distribution of lectin binding sites in human bone marrow. Identification by use of an ultrastructural postembedding technique. *J Submicrosc Cytol Pathol*. 1996;28:537–551.
60. Ha Y, Liu H, Xu Z, et al. Endoplasmic reticulum stress-regulated CXCR3 pathway mediates inflammation and neuronal injury in acute glaucoma. *Cell Death Dis*. 2015;6:e1900.
61. Bricker-Anthony C, Rex TS. Neurodegeneration and vision loss after mild blunt trauma in the C57Bl/6 and DBA/2J Mouse. *PLoS One*. 2015;10:e0131921.
62. Clark RA. Basics of cutaneous wound repair. *J Dermatol Surg Oncol*. 1993;19:693–706.
63. Mazure A, Grierson I. In vitro studies of the contractility of cell types involved in proliferative vitreoretinopathy. *Invest Ophthalmol Vis Sci*. 1992;33:3407–3416.
64. Luttrull JK, Musch DC, Mainster MA. Subthreshold diode micropulse photocoagulation for the treatment of clinically significant diabetic macular oedema. *Br J Ophthalmol*. 2005; 89:74–80.
65. Vujosevic S, Bottega E, Casciano M, Pilotto E, Convento E, Midena E. Microperimetry and fundus autofluorescence in diabetic macular edema: subthreshold micropulse diode laser versus modified early treatment diabetic retinopathy study laser photocoagulation. *Retina*. 2010;30:908–916.
66. Park SS, Moisseiev E, Bauer G, et al. Advances in bone marrow stem cell therapy for retinal dysfunction. *Prog Retin Eye Res*. 2017;56:148–165.
67. Sramek C, Mackanos M, Spitler R, et al. Non-damaging retinal phototherapy: dynamic range of heat shock protein expression. *Invest Ophthalmol Vis Sci*. 2011;52:1780–1787.
68. Fort PE, Lampi KJ. New focus on alpha-crystallins in retinal neurodegenerative diseases. *Exp Eye Res*. 2011;92:98–103.
69. Ousman SS, Tomooka BH, van Noort JM, et al. Protective and therapeutic role for alphaB-crystallin in autoimmune demyelination. *Nature*. 2007;448:474–479.
70. Adamis AP. Is diabetic retinopathy an inflammatory disease? *Br J Ophthalmol*. 2002;86:363–365.
71. Chidlow G, Shibeeb O, Plunkett M, Casson RJ, Wood JP. Glial cell and inflammatory responses to retinal laser treatment: comparison of a conventional photocoagulator and a novel, 3-nanosecond pulse laser. *Invest Ophthalmol Vis Sci*. 2013;54: 2319–2332.
72. Wood JP, Shibeeb O, Plunkett M, Casson RJ, Chidlow G. Retinal damage profiles and neuronal effects of laser treatment: comparison of a conventional photocoagulator and a novel 3-nanosecond pulse laser. *Invest Ophthalmol Vis Sci*. 2013;54:2305–2318.
73. Chehade L, Chidlow G, Wood J, Casson RJ. Short-pulse duration retinal lasers: a review. *Clin Exp Ophthalmol*. 2016; 44:714–721.
74. Jobling AI, Guymer RH, Vessey KA, et al. Nanosecond laser therapy reverses pathologic and molecular changes in age-related macular degeneration without retinal damage. *FASEB J*. 2015;29:696–710.
75. Ambati J, Atkinson JP, Gelfand BD. Immunology of age-related macular degeneration. *Nat Rev Immunol*. 2013;13:438–451.
76. Inagaki K, Shuo T, Katakura K, Ebihara N, Murakami A, Ohkoshi K. Sublethal photothermal stimulation with a micropulse laser induces heat shock protein expression in ARPE-19 Cells. *J Ophthalmol*. 2015;2015:729792.
77. Guymer RH, Brassington KH, Dimitrov P, et al. Nanosecond-laser application in intermediate AMD: 12-month results of fundus appearance and macular function. *Clin Exp Ophthalmol*. 2014;42:466–479.
78. Qi X, Pay SL, Yan Y, et al. Systemic injection of RPE65-programmed bone marrow-derived cells prevents progression of chronic retinal degeneration. *Mol Ther*. 2017;25:917–927.
79. Kase S, He S, Sonoda S, et al. alphaB-crystallin regulation of angiogenesis by modulation of VEGF. *Blood*. 2010;115:3398–3406.
80. Wong WT. Microglial aging in the healthy CNS: phenotypes, drivers, and rejuvenation. *Front Cell Neurosci*. 2013;7:22.
81. Yu AK, Merrill KD, Truong SN, Forward KM, Morse LS, Telander DG. The comparative histologic effects of subthreshold 532- and 810-nm diode micropulse laser on the retina. *Invest Ophthalmol Vis Sci*. 2013;54:2216–2224.
82. Lavinsky D, Cardillo JA, Melo LA Jr, Dare A, Farah ME, Belfort R Jr. Randomized clinical trial evaluating mETDRS versus normal or high-density micropulse photocoagulation for diabetic macular edema. *Invest Ophthalmol Vis Sci*. 2011; 52:4314–4323.
83. Roider J, Liew SH, Klatt C, et al. Selective retina therapy (SRT) for clinically significant diabetic macular edema. *Graefe's Arch Clin Exp Ophthal*. 2010;248:1263–1272.
84. Luttrull JK, Sramek C, Palanker D, Spink CJ, Musch DC. Long-term safety, high-resolution imaging, and tissue temperature modeling of subvisible diode micropulse photocoagulation for retinovascular macular edema. *Retina*. 2016;36:1658–1663.
85. Luttrull JK, Chang DB, Margolis BW, Dorin G, Luttrull DK. Laser resensitization of medically unresponsive neovascular age-related macular degeneration: efficacy and Implications. *Retina*. 2015;35:1184–1194.
86. Al Mheid I, Hayek SS, Ko YA, et al. Age and human regenerative capacity: impact of cardiovascular risk factors. *Circ Res*. 2016;119:801–809.
87. Niederseer D, Steidle-Kloc E, Mayr M, et al. Effects of a 12-week alpine skiing intervention on endothelial progenitor cells, peripheral arterial tone and endothelial biomarkers in the elderly. *Int J Cardiol*. 2016;214:343–347.
88. Povsic TJ, Sloane R, Pieper CF, et al. Endothelial progenitor cell levels predict future physical function: an exploratory analysis from the VA Enhanced Fitness Study. *J Gerontol A Biol Sci Med Sci*. 2016;71:362–369.

Investigative Ophthalmology & Visual Science